# Observation of current-discontinuity lines in type-II superconductors

Th. Schuster, M. V. Indenbom,* M. R. Koblischka,† H. Kuhn, and H. Kronmüller
*Max-Planck-Institut für Metallforschung, Institut für Physik, Heisenbergstrasse 1, 70569 Stuttgart, Germany*
(Received 25 June 1993)

In this paper, magneto-optical observations and analyses of skeleton structures of flux distributions in type-II superconductors are presented. It will be shown that these structures are formed by lines where the critical current is bending. Such lines are a characteristic feature of a vortical vector field if the absolute value of the vector is constant as for the current distribution in a type-II superconductor in the full critical state. Thin samples offer enhanced sensitivity to observe these current discontinuity lines magneto-optically due to two facts: The Meissner phase contracts to these lines and remains there up to fields, which are higher than the full penetration field $H^*$. At much higher magnetic fields, when the Meissner phase has vanished, the logarithmic infinity of the magnetic flux density at these lines leads to sufficiently high contrast. The positions of the discontinuity lines are not affected directly by particular defects, but are determined by the shape of the sample. Because the vortices are not able to cross these lines, the current discontinuity lines determine the flux distribution in the superconductor like a magnetic skeleton. An analysis of the observed structures yields characteristic parameters of the sample as anisotropy, inhomogeneity, or irradiation-induced enhancement of the critical current density. Additionally, the presence of defects allows the observation of the direction of flux motion and, thus, to visualize directly the current distribution. A strong concentration of flux motion near defects without any peculiarities of the current and magnetic flux distribution can be predicted using the consideration presented in this paper.

## I. INTRODUCTION

The magneto-optical Faraday effect allows one to study the local flux distribution in superconductors. Using the Faraday effect of europium chalcogenide thin films which are deposited directly onto the sample surface the maximum attainable resolution of about 1 $\mu$m is obtained.[1–3] This high-resolution Faraday effect (HRF) technique was successfully applied to high-$T_c$ superconductors.[3,4] Especially for the high-$T_c$ superconductors, a new technique using the Faraday effect of garnet films has been developed.[5,6] With this method a very high magnetic field sensitivity of about $10^{-2}$ mT and a spatial resolution of some 5 $\mu$m is achieved within the whole temperature range relevant for the high-$T_c$ materials.

By means of the two methods, new results on the understanding of flux behavior in type-II superconductors were obtained. For thin samples with thicknesses much smaller than the sample width and with the external magnetic field applied perpendicular to the sample surface, the following results have been obtained.

(1) In superconducting thin films the magnetic flux density gradient $\partial B_z/\partial x$ ($x$ denotes the coordinate parallel to the sample surface, $z$ that one perpendicular to the sample surface) is much smaller than the gradient required to explain the supercurrent density $\mathbf{j}_c = (1/\mu_0)\,\mathrm{curl}\,\mathbf{B}$.[7,8] This is due to the strong field line curvature which was observed directly in Ref. 9. The magnetic flux density gradient $\partial B_z/\partial x$ however, is the only one to be detected magneto-optically. Using a self-consistent numerical procedure, Theuss *et al.*[10] were able to calculate the current distributions within circular patterned samples from magneto-optically measured flux density gradients $\partial B_z/\partial x$.

(2) In superconducting thin film samples exists a barrierlike flux penetration[8,11] due to the special distribution of Meissner currents.[12]

(3) For complicated sample geometries, the magnetic flux does not penetrate evenly from the sample edges. Instead, the flux penetration takes place mainly in the middle of straight sample edges, whereas at the sample corners no flux penetration is observed.[6,13,14]

(4) In the remanent state, flux lines with opposite sign are generated at the sample edges by the stray field of the pinned vortices.[7,15]

Just recently, the influence of anisotropy on flux penetration was observed at external magnetic fields applied perpendicular to the $c$ axis of a cubic melt-processed $YBa_2Cu_3O_{7-\delta}$ (YBCO) sample.[16] In particular, magneto-optical techniques provide powerful tools for investigations of time dependent and spatially inhomogenous processes, e.g., the dendritelike flux penetration during heat instabilities, which were carried out on conventional[17] as well as on high-$T_c$ (Ref. 18) superconductors.

To calculate the current density from magneto-optically measured flux density profiles, numerical[10,19–21] and analytical[12,22,23] solutions exist only for thin samples ($d \ll w$ where $d$ is the thickness and $w$ the width of the sample) patterned as circles or long strips, i.e., for one-dimensional problems, and in the case of long prismas ($l \gg R$, where $l$ denotes the length and $R$ is a characteristical length to describe the dimensions of

 

the cross-section perpendicular to $l$). To determine the current densities for geometries more complicated than those mentioned above one has to solve two- or three-dimensional, nonlinear problems of current distributions, which is very eligible and cannot be done rigorously in all cases. Therefore, a simplified method has to be introduced.

For sample geometries different from the circular patterned thin film, the long thin strip or the long prisma, the Meissner currents, i.e., supercurrents lower than the critical current, not only change their value when the external magnetic field is increased, but also their direction. In addition, the distribution of the Meissner currents is not homogenous within the sample, but its value varies up to the value of the critical current. To avoid the difficulties arising with the presence of spatially varying Meissner currents, we consider a sample in the critical state, i.e., with critical current density $j_c$ flowing in the entire sample. Thus, the value of the current density is constant in the whole sample and its direction is given by the condition that the critical current has to flow parallel to the sample edges. Such a model was reviewed by Campbell and Evetts.[24] In this paper we will extend this model and apply it to reproduce complicated flux density distributions, especially in circular patterned and partly irradiated YBCO thin films observed by means of the HRF technique. The critical state is realized by applying high external magnetic fields. In this paper, we will restrict ourselves to experiments using the HRF technique, however, all the results are also valid for the other kinds of observation methods.

The present paper is organized as follows: In Sec. II, a short outline of the HRF technique is presented and a description of the local measurement of critical current densities will be given. In Sec. III, the model itself will be presented and applied to describe the geometry dependence of the flux distributions. Section IV shows the application of the model to determine the critical current densities in partly heavy-ion irradiated YBCO thin film samples. In Sec. V, speculations concerning flux motion are presented. Finally, in Sec. VI, we will summarize our results.

## II. EXPERIMENTAL PROCEDURE

### A. The high-resolution Faraday effect technique

The experiments are performed using the optical cryostat and microscope which is described in detail in Refs. 25 and 26. Direct observations by means of the HRF technique are possible only in the temperature range 5 K $\leq T \leq$ 20 K. The lower-temperature limit is given by the technology of the cryostat, the upper boundary is imposed by the temperature-dependent Verdet constant of the europium chalcogenides.[2,3] In the present paper, we show observations of the Shubnikov phase at a temperature of $T = 5$ K. The images can be observed directly at the microscope or may be transferred to an image-processing system for analyzing purposes.[27] The external magnetic field is generated by a copper solenoid coil producing a maximum field of 0.6 T. First, the calibration technique shown in Ref. 28 is followed. To calibrate the measured intensity $I$ in terms of the local flux density $B_z$, two fixed points are determined: In the Meissner phase at the center of the sample we have $B_z = 0$. Far away from the sample edge on the substrate, the measured intensity corresponds directly to the external field, $\mu_0 H_{\text{ext}}$. Using these fixed points, every intensity measured can be expressed in terms of $B_z$.

The current density can be expressed as

$$\mathbf{j} = (1/\mu_0)\text{curl}\mathbf{B} \ . \tag{1}$$

In the case of a circular sample showing a radially symmetric penetration of the flux follows (in cylindrical coordinates)

$$j_\varphi(r) = (1/\mu_0)\left[\frac{\partial B_z}{\partial r} - \frac{\partial B_r}{\partial z}\right] \ . \tag{2}$$

If the flux distribution in a superconductor is regarded, the two gradients $\partial B_z/\partial r$ and $\partial B_r/\partial z$ yield a maximum current density in the Shubnikov phase where the critical current density $j_c$ is flowing. In this case the current density $j(r)$ must be replaced by $j_c(r)$ in Eq. (2). As shown in Ref. 8, the critical current density is not governed by the flux-density gradient $\partial B_z/\partial r$ but by the gradient $\partial B_r/\partial z$ which is larger by the factor $R/d$ in most regions of the sample. In the case of a thin film with a thickness $d = 500$ nm and a radius $R = 1$ mm the factor $R/d$ is 2000. As the HRF technique allows only a detection of $\partial B_z/\partial r$, a numerical calculation technique of how to obtain the gradient $\partial B_r/\partial z$ was developed in Ref. 10. For these calculations, the current distribution $j(r)$ in the film is approximated by $N$ concentric current loops which are spaced equidistantly so that the measurement is reproduced via the Biot-Savart law. In this model a homogeneous current density distribution in the $z$ direction is assumed. Such an approximation is valid for films with a thickness $d$ lower than the London penetration depth $\lambda_L$. But even for samples with $d > \lambda_L$, such a procedure can be applied, if variations of $B_z$ on the scale of the sample thickness can be neglected. In this case, the determined $j(r)$ data represent an average value of the current density over the sample thickness. To obtain the current distribution $j(r)$ a numerical fit to the flux density profiles $B_z(r)$ is performed. From this fit, the critical current density $j_c$ can be determined as the value of $j(r)$ in the Shubnikov phase.

### B. Sample preparation and irradiation

The $DyBa_2Cu_3O_{7-\delta}$ (DyBCO) single crystals were grown using a self-flux method as described in Ref. 29. This procedure leads to nearly twin-free crystals with a rectangular shape of about 600 × 600 × 15 $\mu$m.

For the experiments carried out on partly irradiated, $c$-axis-oriented thin films, two types of YBCO samples were used. The samples intended for the oxygen irradiation were produced at Siemens Laboratories, Erlangen,

by laser-ablation technique with a film thickness of 300 nm.[30] All other thin film samples were prepared at the University of Erlangen by planar dc sputtering from a sintered stoichiometric YBCO pellet on $SrTiO_3$ substrates heated up to 750 °C.[31] These samples had a thickness of 450 nm and were exposed to irradiation by lead ions.

All thin film samples were patterned chemically to a circular shape with a diameter of 2 mm. To obtain an easier handling in the various experimental stages, the samples were glued onto copper sample holders.

For all heavy-ion irradiations, the beam direction was chosen perpendicular to the sample surface of the thin films and, hence, parallel to the $c$ axis of the materials. The oxygen irradiation was performed at the low-temperature facility of the tandem accelerator at the University of Erlangen. During the irradiation, the samples were cooled with liquid nitrogen and warmed up to room temperature afterwards. The energy of the oxygen ions was chosen to be 25 MeV. The irradiation with 1.0-GeV Pb ions was carried out at GANIL (Caen, France) at room temperature. During the oxygen and lead irradiation, one-half of each thin film sample was covered by a copper absorber and, therefore, not exposed to the heavy-ion beam.

For use with the HRF technique, all samples were coated with an aluminium layer (thickness about 100 nm) to enhance their reflectivity and with the magneto-optical active EuSe thin film (thickness about 250 nm).

## III. THE MODEL

To determine the complete current distibution within a superconducting sample, one has to deal with a complicated arrangement of Meissner currents and critical currents. The density of the Meissner currents is not spatially constant within the superconductor and can be of any value up to the critical current density $j_c$ and the Meissner currents are not fixed in the direction they are flowing in. The calculation of the distribution of Meissner currents is extremely complicated and, therefore, only for the two simplest geometries, the long thin strip and the circular disk, numerical approximations, as well as analytical solutions are available. To avoid the difficulties arising in determining the current distribution in superconducting samples with a geometry different from those mentioned above, only samples in the critical state will be considered where the current density takes the critical value $j_c$ everywhere.

The basic assumption of the critical state model is that magnetic flux can only move into a superconductor if the supercurrents reach the value of the critical current which generally depends on the applied magnetic field. If a superconductor is completely penetrated by magnetic flux at a magnetic field $H \gg H^*$ where $H^*$ denotes the full penetration field, the dependence of $j_c$ on the external magnetic field no longer affects the current distribution within the sample, but only the absolute value of the critical current density. If $j_c = \text{const}$, this constant current distribution holds in the whole range $H \geq H^*$. In the other case, i.e., if the sample is not fully penetrated by magnetic flux, a variation of the external magnetic field yields a change in the current distribution within the whole superconductor. It means therefore a strong simplification of this complex problem if we consider the entire sample to be in the critical state. However, these assumptions provide a useful tool to point out the essential characteristics of the geometry dependent flux distribution observed by means of the HRF technique. An important point of such a distribution of the critical current density is the existence of lines where the direction of flow of $j_c$ is changed sharply. Campbell and Evetts[24] demonstrated the appearance of such a line in the vicinity of an extended circular cavity near the edge of a superconductor as presented in Fig. 1. The critical current is flowing always parallel to the sample edges due to the continuity equation and because $j_c$ is constant over the entire superconductor. The critical current density, symbolized by equidistant current lines, is flowing parallel to the sample edge located at the bottom of Fig. 1. When the magnetic flux penetrating from the sample edge reaches the cavity, the current lines have to form sharp bends in order to flow around the hole on arcs of concentric circles, still fulfilling the condition of equidistant current lines. The bending points which are given by the intersection of the circles with the current lines parallel to the sample edge form a parabola described by $r = 2R/(1-\sin\varphi)$. Here, $r$ and $\varphi$ are the polar coordinates and $R$ denotes the radius of the cavity whose center is located in the origin. Campbell and Evetts denoted the curves on which the bending points lie by lines of current discontinuity. In the following, we will refer to these curves as $d$ lines. The $d$ lines are a characteristic feature of critical currents flowing in type-II superconductors. This is a particular case of the general problem of a vector field with constant size of the vector and with zero divergence as developed for soft magnetic materials.[32] We will return to the situation presented in Fig. 1 again in Sec. V.

Whereas Campbell and Evetts regarded a long cylinder with the external magnetic field oriented parallel to its

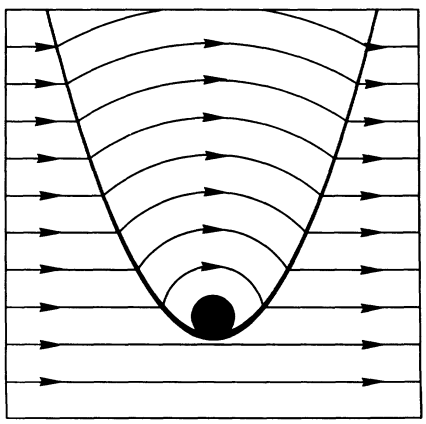

FIG. 1. Schematical drawing of the current distribution in the vicinity of a cylindrical cavity near the edge of a superconductor. The sample edge is located at the bottom of the figure. The spatially constant current density $j_c$ is symbolized by equidistant current lines and the arrows indicate the direction of the current.

axis, we shall consider thin film samples with the external magnetic field applied perpendicular to the sample surface; in thin superconductors the $d$ lines can be observed magneto-optically due to the appearance of a logarithmic infinity of the magnetic flux density at these lines. To explain the main features of the $d$ lines and the conditions of how they can be observed, we consider a thin long superconducting strip with a length-to-thickness ratio $l/d$ of at least 7 and a rectangular sample ($l/d \approx 1.5$) both observed by means of the HRF technique.

### A. The long thin strip

In Fig. 2(a), the flux distribution measured at a thin YBCO strip ($d$ = 300 nm, $w$ = 100 $\mu$m) is shown in a full critical state. The dark lines denote the edges of the sample and, therefore, are not influenced by the external magnetic field. These lines are not shown in the corresponding flux density profile presented in Fig. 2(b). This figure shows also the current directions and the $d^+$ and $d^-$ lines. In the following, we will use the plus sign for the $d$ lines due to the geometry dependent flux penetration and the minus sign for the lines at sample edges and, as will be shown in Sec. IV, at structural boundaries in the sample. The good visibility of both the $d^+$ and the $d^-$ lines is due to the logarithmic infinity of the flux density, which we will discuss now for the sample edges and the center of the strip. Writing the current distribution $\mathbf{j} = (0, \pm j_c, 0)$ for the two halves of the sample separated by the $d^+$ line where $j_c$ flows in opposite directions (i.e., $+j_c$ and $-j_c$) we get the flux density published by Baczewski *et al.*:[7]

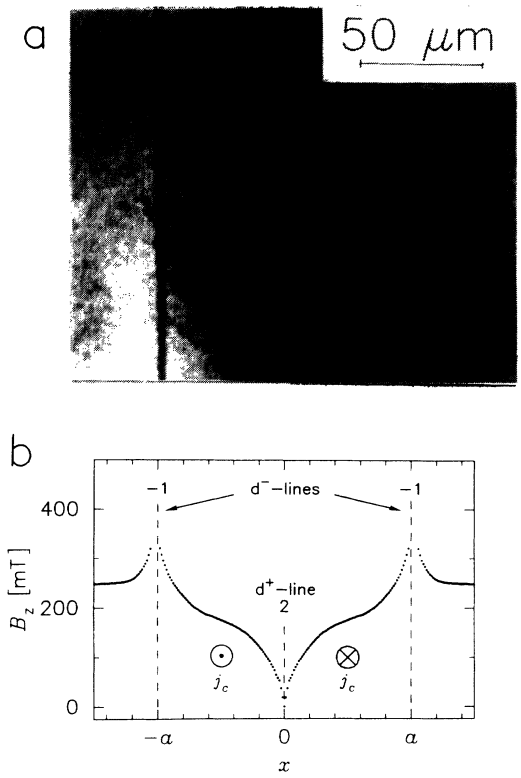


FIG. 2. (a) Direct observation of the flux distribution in a long thin superconducting strip at an external magnetic field of $\mu_0 H_{ext}$ = 246 mT. The observation temperature is $T$ = 5 K. The dark lines indicate the sample edges. (b) Flux-density profiles $B_z(x)$ obtained from the image presented in (a); $2a$ denotes the sample width. The influence of the dark lines at the sample edges $a = \pm$ 0.5 on the flux density profiles is neglected. The position of the $d^+$ line in the middle of the sample and of the $d^-$ lines at the sample edges and their values $K_l$ = 2 and $K_l$ = −1, respectively, are indicated. In addition, the direction of flow of the critical current density $j_c$ in each half of the sample is marked by ⊙ for the direction of flow out of the plane of drawing and by ⊗ for the direction of flow into this plane.

$$B_z = \pm \frac{\mu_0}{2\pi} j_c d \ln \left| \frac{x^2}{a^2 - x^2} \right| . \tag{3}$$

Here, $a$ denotes half the width of the strip and $d$ the thickness of the sample. The $\pm$ sign indicates that the critical current density reverses its direction of flow in both halves of the sample when the external magnetic field is lowered. The two limits $x \to \pm a$ and $x \to 0$ yield the values −1 and 2 for the line intensity factor $K_l$ of the $d^-$ and $d^+$ line, respectively, near the logarithmic infinity of the flux density

$$B_z = \pm K_l \frac{\mu_0}{2\pi} j_c d \ln(\delta x) , \tag{4}$$

where $\delta x$ denotes the distance from the corresponding $d$ line. These values can be explained also by regarding the currents flowing in the vicinity of the respective $d$ lines. In the center of the strip, the value $K_l = 2$ is due to the addition of the magnetic fields of the currents flowing in inverse directions. In contrast, the current flows only on one side of the $d^-$ lines at the sample edges. The sign of $K_l$ is always positive at the $d^+$ lines and negative at the $d^-$ lines in all cases considered in this work.

Before the critical state is reached the Meissner phase remains at the position of the $d^+$ line. Its width $\Delta x_M$ is obtained from the analytical solution which describes the whole process of magnetization:[12]

$$\Delta x_M \sim \exp\left[ -\frac{H_{ext}}{H_c} \right] , \tag{5}$$

in the range $H_c = j_c d/\pi \ll H_{ext} \leq H^* \approx H_c \ln(a/d)$. If $H_{ext}$ exceeds $H^*$, the Meissner phase vanishes, but the $d^+$ line marking the center of the former Meissner phase can still be observed as a dark line due to the logarithmic infinity of the magnetic flux density $B_z$ at this line.

### B. The rectangle

Figure 3(a) presents the flux distribution of a nearly rectangular DyBCO single crystal with a thickness of 15 $\mu$m at an external magnetic field of $\mu_0 H_{ext}$ = 340 mT. The $d^+$ line shows the typical shape of a double $Y$, disturbed by some small crystal defects at the bottom of the image. The flux is found to penetrate the sample not starting from the corners of the sample as is often

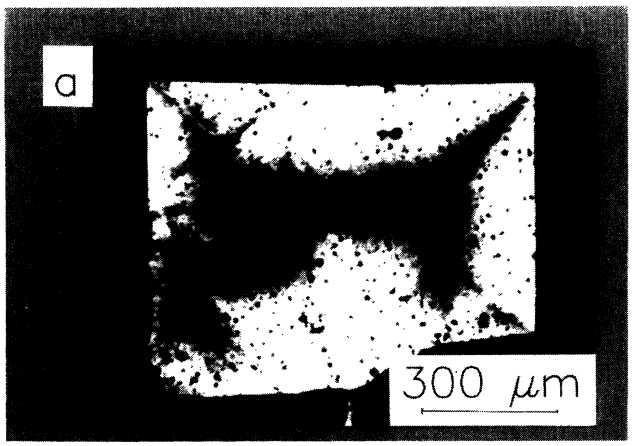


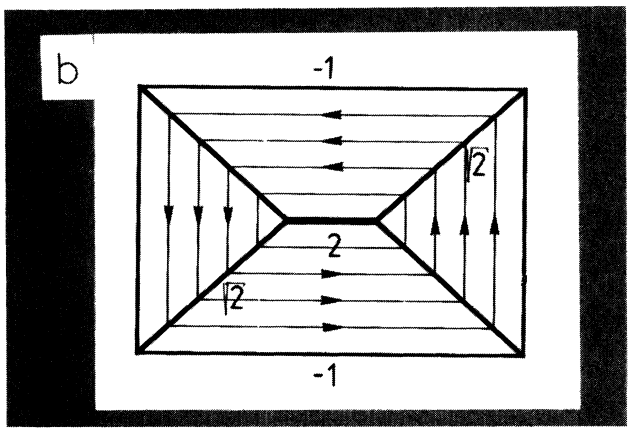


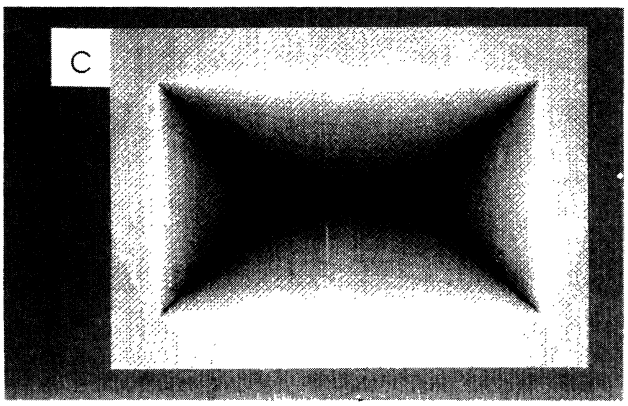


FIG. 3. (a) Flux distribution obtained on a nearly rectangular DyBCO single crystal at an external magnetic field of $\mu_0 H_{\text{ext}} = 512$ mT at $T = 5$ K. The magnetic flux penetrates the sample preferably starting from the middle of each sample edge thus leading to the formation of a Meissner phase shaped as a double $Y$. (b) Current distribution in a rectangular sample. Again, the arrows indicate the direction of flow of the constant current density symbolized by equidistant current lines. The numbers indicate the values of $K_l$ of the respective $d$ lines. The different $K_l$ values for the $d^+$ lines in the center of the sample and along the bisection lines are symbolized by a variable linewidth. (c) Flux distribution calculated from the current distribution presented in (b) via the Biot-Savart law.

naively expected. To show this in more detail, the distribution of the critical current densities and the $d$ lines are presented in Fig. 3(b) for a rectangular sample in the critical state. The critical current densities flowing parallel to the sample edges and, thus, the $d^+$ lines, which in Fig. 3(a) represent the rest of the Meissner phase, form the shape of a double $Y$. The numbers near the $d$ lines indicate the corresponding values of $K_l$ and, thus, characterize the field distribution. Regarding the different $K_l$ values of the $d^+$ lines in Fig. 3 we obtain, for the width of the Meissner phase using Eqs. (4) and (5) in this general case,

$$\Delta x_M \sim \exp\left[-\frac{2}{K_l}\frac{H_{\text{ext}}}{H_c}\right] . \tag{6}$$

This indicates that the $K_l$ value in the center of the sample is larger than at the $d^+$ lines along the bisection lines, particularly obvious in the upper right half of the image. To explain this difference, we regard again Eq. (3). Along the $d^+$ lines, we split the current directions in parallel and perpendicular components. The value of the $d^+$ line is governed by the component parallel to the $d^+$ line itself. The $B_z$ component near the $d^+$ line is described by Eq. (4), using

$$K_l = 2\cos(\vartheta/2) . \tag{7}$$

The angle $\vartheta$ is defined by the declination of the current lines at the bending points. In the case of a rectangular sample, we obtain for the $d^+$ lines the values $K_l = \sqrt{2}$ (bisection lines) and $K_l = 2$ (center of the sample). These values are visible in the magneto-optic images as width of the Meissner areas or, at higher magnetic fields $H_{\text{ext}} \gg H^*$ as the intensity of the $d^+$ line, respectively. The value $K_l = -1$ for the $d^-$ line at the sample edges is due to the same reasons as discussed with the thin strip.

Figure 3(c) presents the calculated distribution of the magnetic field in the critical state. This calculation was performed by using the current distribution shown in Fig. 3(b) and the Biot-Savart law. The good agreement of the calculated distribution with the obtained images is clearly visible, particularly at the lines at 45° to the center of the sample the flux distribution is reproduced nearly exactly by the model. Also, the reduction of intensity due to superposition of $d^+$ and $d^-$ lines in the corners of the samples is clearly visible. The logarithmic infinity of the magnetic field exists only in thin samples and, hence, the $d$ lines are not so clearly visible in bulk samples. However, the $d^+$ line always forms the shape of a double $Y$ in a rectangular superconductor, regardless whether it is a thin plate or an extended parallelepiped.

Figure 4(a) shows the flux distribution of the same DyBCO single crystal as already shown in Fig. 3(a) in the remanent state after applying an external magnetic field of $\mu_0 H_{\text{ext}} = 550$ mT and subsequently reducing it to zero. In Fig. 4 (b), we have applied an external magnetic field of $\mu_0 H_{\text{ext}} = -300$ mT (i.e., in opposite direction) to the state presented in Fig. 4(a). This series of images was chosen to show once more interesting aspects of the $d^+$ and $d^-$ lines, which are summarized in the following.

(1) In the remanent state obtained by applying a mag-

netic field $H_{ext} > 2H^*$ the critical current density $j_c$ changes its direction of flow and, thus, the $d^+$ lines are imaged as bright lines, whereas the $d^-$ lines appear dark. However, the values of $K_l$ remain unchanged. The opposite contrast of the $d$ lines is clearly visible in Fig. 4(a). In Fig. 4(b), the termination of the process of reversing the contrasts at the $d^+$ line is demonstrated by applying an external magnetic field of opposite polarity to the remanent state.

(2) The vortices are not able to cross the $d^+$ lines, because the flux on either side flows towards or away from this line. This is clearly demonstrated by the Meissner phase squeezing towards the $d^+$ line within a thin sample.

(3) The position of the $d^+$ lines is defined by the geometry of the sample. In all magneto-optical experiments we never observed any motions of these lines, in contrast to the measurements published by Brawner *et al.*[33] This behavior is clearly demonstrated in Fig. 4(b).

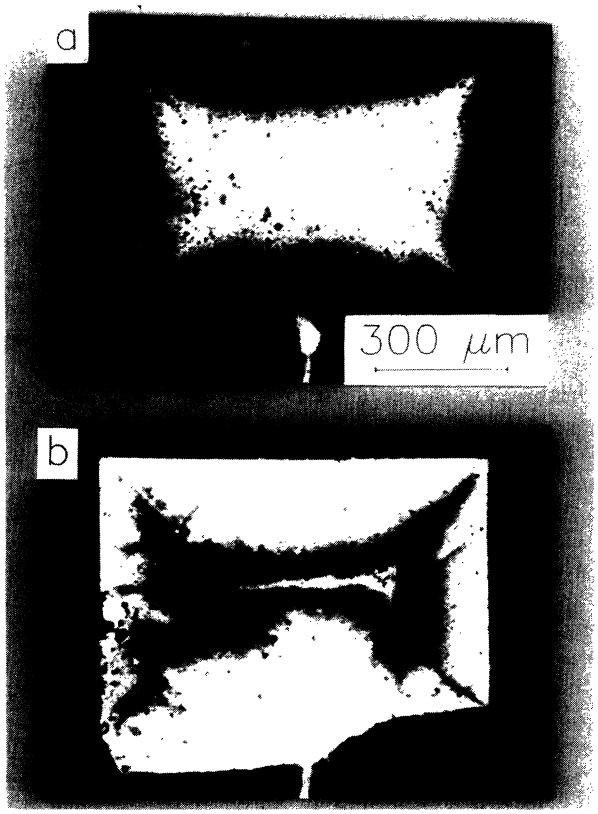


FIG. 4. Remanent state of the DyBCO single crystal presented in Fig. 3(a). (a) Remanent state after applying an external field of $\mu_0 H_{ext} = 512$ mT and subsequently lowering to 0 mT. In the remanent state the $d^+$ line is imaged bright, whereas the $d^-$ line (white arrow) at the sample edge is hardly visible. (b) Flux distribution obtained from the remanent state presented in (a) while applying an external magnetic field of $\mu_0 H_{ext} = -300$ mT in reverse direction. The $d^+$ line with the shape of a double $Y$ is clearly visible as a bright line in the center of the sample.

## IV. APPLICATION OF THE MODEL

In this part we apply this model to obtain the critical current densities in partly heavy-ion irradiated YBCO thin film samples. The results obtained by using a numerical fitting procedure to the measured flux density profiles $B_z(r)$ were presented in detail in Ref. 34. A short outline of the irradiation procedure is given in Sec. II. Here, we focus our attention on the current distributions in such samples.

The principle of the method shall be illustrated by a circular patterned YBCO film which was irradiated with 1.0-GeV lead ions at a fluence of $\phi t = 9.0 \times 10^{10}$ ions/cm$^2$. Only the left half of the sample was exposed to the irradiation while covering the other part with a copper shield. As pointed out earlier,[34] this technique allows the determination of changes of the critical current densities under the same experimental conditions.

The flux distribution of this sample during application of an external magnetic field of $\mu_0 H_{ext} = 273$ mT is presented in Fig. 5(a). The asymmetry of the magnetic flux distribution indicates a small difference in the critical current densities in the two areas. Figure 5(b)

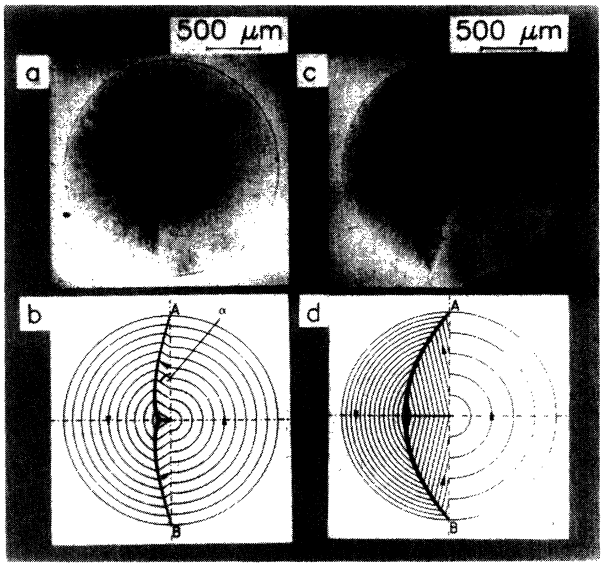


FIG. 5. (a) Flux distribution obtained from a partly irradiated YBCO thin film at an external magnetic field of $\mu_0 H_{ext} = 273$ mT. The left part of the film was irradiated with 1.0-GeV lead ions at a fluence of $\phi t = 9.0 \times 10^{10}$ ions/cm$^2$. The asymmetric flux distribution due to the irradiation-induced enhancement of the critical current density is clearly visible. (b) Current distribution in the thin film presented in (a). The constant critical current density in each half of the sample is symbolized by equidistant concentric circles. The thickness of the $d^+$ line indicates the value of $K_l$ which becomes a maximum at the center of the $d^+$ line. (c) Flux distribution obtained from a YBCO thin film at an external magnetic field of $\mu_0 H_{ext} = 273$ mT. The left half of the sample was irradiated with 1.0-GeV lead ions at a fluence of $\phi t = 30.0 \times 10^{10}$ ions/cm$^2$ . The difference in the critical current densities in both parts is apparently larger than in the case presented in (a). (d) Current distribution in the sample presented in (c).

shows the corresponding current distributions obtained from our model. The difference in the two critical current densities, $j_c(0)$ (unirradiated area) and $j_c(\phi t)$ (irradiated area), is visualized by different densities of current lines in the two areas. In the unirradiated part of the sample (right), the critical current density $j_c(0)$ is flowing parallel to the edge, i.e., on concentric circles, as in an ideal circular patterned film. At the diameter dividing the irradiated area from the unirradiated one (left), the current lines have to bend to the angle $\alpha$ according to

$$j_c(0) = j_c(\phi t) \sin \alpha \ . \tag{8}$$

Thus, the concentric circles go over into a denser set of parallel current lines. Near the left sample edge, the current lines symbolizing $j_c(\phi t)$ are also forming concentric circles. The $d^+$ line follows a curve through the intersection points of the circles and the straight lines and is given by

$$r = \frac{R\,[1 - \sin \alpha]}{1 - \sin\,(\alpha - \varphi)} \ . \tag{9}$$

$r$ and $\varphi$ are the polar coordinates and $R$ denotes the radius of the sample.

The factor $j_c(\phi t)/j_c(0)$, i.e., the irradiation-induced enhancement of $j_c$, can be varied until the flux distribution found in the experiment is obtained. Comparison of the curves calculated from Eq. (9) with the shape of the remaining Meissner region allows us to determine the angle $\alpha$, and hence, the current ratio $j_c(\phi t)/j_c(0)$. On the sample presented in Fig. 5(a), this procedure yields a current ratio of $j_c(\phi t)/j_c(0) = 1.2$. The $d^-$ lines at the sample edges and at the boundary region between the two areas along the line $AB$ are spared out in Fig. 5(b) for clarity. The $d^-$ lines at the sample edges have a value of $K_l = -1$ in the unirradiated area and the value $j_c(\phi t)/j_c(0) = -1.2$ in the irradiated area since $j_c$ is normalized to $j_c(0) = 1$. The boundary is a $d^-$ line with

$$K_l = -\,[j_c(\phi t)/j_c(0)] \cos \alpha = -0.7 \ .$$

In this case the $d^-$ line is not located at a sample edge. Figure 5(c) gives the flux distribution at an external magnetic field of $\mu_0 H_{\rm ext} = 273$ mT on a sample irradiated with 1.0-GeV lead ions and a fluence $\phi t = 30.0 \times 10^{10}$ ions/cm$^2$. Figure 5(d) shows the corresponding current distribution and the $d^+$ line. The ratio $j_c(\phi t)/j_c(0)$ for the current-induced enhancement of the critical current density is found to be 4.6 which is in good agreement with the value $j_c(\phi t)/j_c(0) = 5.1$ obtained by the numerical fitting procedure of Ref. 34. The different ratios 1.2 and 4.6 influence the position of the $d^+$ line which is found to move deeper into the irradiated area at larger differences in $j_c$, and also the $K_l$ values of the $d^+$ and $d^-$ lines are changed. Here, the $d^-$ lines at the sample edges have the values $K_l = -1$ (unirradiated area) and $K_l = -4.6$ (irradiated area) and also $K_l = -4.6$ at the boundary area. Due to the larger difference in the critical current densities $j_c(\phi t)/j_c(0) = 4.6$, the $d^-$ lines are more clearly visible in the irradiated part of the sample presented in Fig. 5(c) than in the case of Fig. 5(a).

To discuss the shape of the $d^+$ lines in partly irradiated disks, we show another flux distribution which allows a comparison of $K_l$ of two $d^+$ lines formed by different current densities within one sample. In Fig. 6(a), a YBCO thin film is presented at $\mu_0 H_{\rm ext} = 13$ mT, which was irradiated with 25-MeV oxygen ions at a fluence of $\phi t = 6.0 \times 10^{14}$ ions/cm$^2$.

In Fig. 6(b), the magnetic flux distribution during application of an external magnetic field of $\mu_0 H_{\rm ext} = 273$ mT is presented. It is clearly visible that two $d^+$ lines are formed showing the presence of a weak link between the two parts of the sample. This leads to a *third* critical current density $j_c(b)$ through the boundary. In this notation, the argument $b$ indicates the current flowing through the boundary. The critical current density $j_c(b)$ is smaller than the two other ones, $j_c(0)$ and $j_c(\phi t)$. The appearance of this third critical current density is due to an irradiation-induced dilatation of volume of the substrate. At large fluences, the irradiated part of the substrate expands and mechanical tensions are induced within the

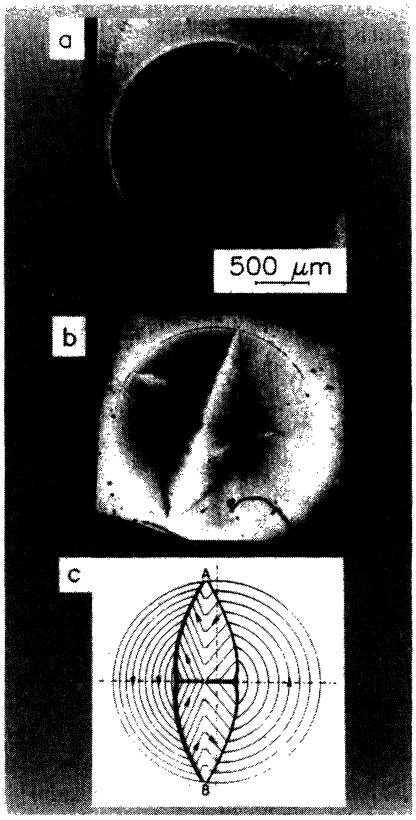


FIG. 6. (a) Flux distribution in an oxygen irradiated YBCO thin film at an external magnetic field of $\mu_0 H_{\rm ext} = 27$ mT. The left half was irradiated at a fluence of $\phi t = 6.0 \times 10^{14}$ ions/cm$^2$. The flux penetration along the division line between the irradiated and unirradiated part of the sample due to mechanical tension in the boundary region is clearly visible. (b) The same sample at an external magnetic field of $\mu_0 H_{\rm ext} = 273$ mT. The formation of the $d^+$ lines due to the irradiation and due to the defect in the upper left part of the sample are clearly visible. (c) Current distribution of the situation presented in (b).

boundary region which influence also the YBCO layer thus leading to a reduction of $j_c$.

Figure 6(c) shows the corresponding current distribution. From this image, the three different critical current densities can be deduced. From Figs. 6(b) and 6(c), both current ratios $j_c(0)/j_c(b)$ and $j_c(\phi t)/j_c(0)$ will be determined in the following. The $d^+$ line is found on a curve as described by

$$r_i = \frac{R[1-\sin(\alpha_i-\varphi_{0i})]}{1-\sin(\alpha_i-\varphi)}, \quad i=1,2\ . \tag{10}$$

$\varphi_{0i}$ is a correction angle which enters since the border between the irradiated and the unirradiated area is not exactly located in the center of the sample. This angle $\varphi_{0i}$ is enclosed by the line through the sample center and the intersection point of the $d^+$ line with the sample edge and by the border line itself. The index 1 denotes the irradiated area and the index 2 the unirradiated area of the sample.

The ratio $j_c(0)/j_c(b)$ of the current densities was obtained in analogy to the formerly described determination of $j_c(\phi t)/j_c(0)$ by variation of the angles $\alpha_i$ and $\varphi_{0i}$ and by comparison with the magneto-optically measured flux distribution. The ratio $j_c(0)/j_c(b)$ is found to be 1.65 from this model. The irradiation-induced enhancement of the critical current densities is then calculated to 1.60 using the relationship

$$\frac{j_c(\phi t)}{j_c(0)} = \frac{\sin\alpha_2}{\sin\alpha_1} \tag{11}$$

deduced from the condition of continuity of the currents.

A qualitative description of the $d^+$ lines in Fig. 6(b) yields the following.

(1) Since in Eq. (4) $B_z \sim K_l j_c$ and the value of $K_l$ is given by the width of the Meissner phase, the irradiation-induced enhancement of $j_c$ is visible as a broader $d^+$ line in the irradiated area.

(2) Equation (7) yields $K_l \sim \cos(\vartheta/2)$, where, in our case, $\vartheta$ is defined as $90^\circ + \alpha - \varphi$, and is reducing towards the center of the $d^+$ line since $\varphi$ is continuously growing. Regarding Eq. (7), one expects a reduction of $K_l$ from the center of the $d^+$ line to the sample edge. This is clearly visible for all $d^+$ lines in Fig. 6(b).

The value of the third critical current density can be estimated from the measured depth of the initial flux penetration, $\Delta x(H)$, in Fig. 6(a). Here, large areas in both regions are remaining in the Meissner state whereas the flux penetrates the sample in the boundary region up to a distance of $\Delta x$. The Meissner state in a circular disk allows for a maximum shielding current density[12]

$$j_M(r) = \frac{\pi H_{\rm ext} r}{d\,(R^2-r^2)^{1/2}}\ . \tag{12}$$

Here, $R$ denotes the sample radius, $d$ the sample thickness, and $r$ the polar coordinate with the center of the sample as zero point. Since a superconductor can carry only a loss-free current $j < j_c$, one has $j_{M,\max}(r) = j_c$. Near the boundary the critical current density will be reached earlier than in the other parts of the sample, and the flux will penetrate into the sample to the depth $\Delta x$ where $j_c(b) = j_M(r)$. So $j_c(b)$ can be estimated from Eq. (12):

$$j_c(b) \approx \frac{\pi H_{\rm ext}}{\sqrt{2}d} \cdot \left(\frac{R}{\Delta x}\right)^{1/2}\ . \tag{13}$$

Using the known data for $H_{\rm ext}$, $d$, $R$, and $\Delta x$ yields $j_c(b) = 1.7\times10^7$ A/cm$^2$. Together with the critical current density $j_c(0) = 4.0\times10^7$ A/cm$^2$, which was determined using our numerical fitting procedure of Sec. II, we obtain a factor $j_c(0)/j_c(b) = 2.3$.[34]

The two values obtained by the different techniques, $j_c(\phi t)/j_c(0) = 1.85$ [numerical fitting to the measured $B_z(r)$-profiles] and $j_c(\phi t)/j_c(0) = 1.60$ (this model), are in good agreement with each other. The same conclusion applies to the other ratio $j_c(0)/j_c(b)$ determined to be 2.3 (fitting) or 1.65 (model).

## V. SUPPLEMENTARY SPECULATIONS

In this section we demonstrate the influence of the defect structure within a sample on the visualization of flux motion. In the upper left part of the sample presented in Fig. 6(b) the formation of a parabolic $d^+$ line at a defect is visible. At this defect, the magnetic flux penetrates into the superconductor similarly to the situation described in Fig. 1. Figure 7 shows the current distribution and the $d^+$ line in the vicinity of a linear defect. Here, as well as in Fig. 1, the constant current density is visualized by equidistant current lines. Near the defect, the $d^+$ line is formed as straight lines intersecting the current lines at an angle of 45° and then passes over to the parabola described earlier in this work (cf. Fig. 1). The thickness of the $d^+$ line indicates the value of $K_l$. The parabolic $d^+$ line is a characteristical feature of the flux distribution in the vicinity of defects not only near the edge but also in the volume of a superconductor. The two branches of the parabola show the direction of motion of the vortices, which is perpendicular to the current lines. In Fig. 5(a),

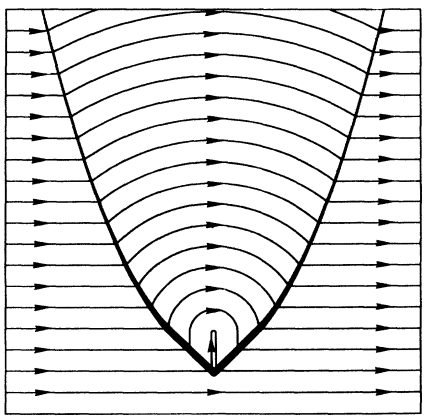

FIG. 7. Current distribution in the vicinity of a linear defect near the edge of a superconductor. The sample edge is located at the bottom of the figure.

the flux motion in the whole sample can be seen due to the presence of a large number of defects. Thus, *we are able to visualize the current distribution within thin films directly by means of the HRF technique.* The flux motion observed in Fig. 5(a) is in excellent agreement with the theoretical current distribution presented in Fig. 5(b).

As for the critical state, we want to point out another interesting feature of flux motion as a consequence of the situation presented in Fig. 1. Figure 8 shows the defect area from Fig. 1 in more detail. The solid arrows, at the current lines, indicate the direction of flow of the critical current around the defect symbolized by the dot matrix. The parabolic $d^+$ line is plotted using a variable line width to indicate the $K_l$ value. How can the flux lines enter the region enclosed by the parabola?

The vortices enter the sample at the edge located at the bottom of Fig. 8 and move perpendicular to the current lines as indicated by the open arrows. Thus, only at the vertex of the parabola, due to the superposition with the $d^-$ line, the $d^+$ line becomes permeable for the flux lines. This means all vortices which are located inside the parabola have to cross the $d^+$ line at its vertex, and, hence, in Fig. 8 many more vortices have to enter the sample at point 1 than at point 2. This is symbolized in Fig. 8 by solid arrows of different size pointing into the direction where different fluences of flux lines move into the sample. So, much stronger flux motion should take place in channel 1 than in channel 2. Channel 1 is a distingiushed place for the nucleation of a thermal jump. Note that this explanation of thermal jumps does not require the presence of any peculiarities of the current and magnetic field distribution.

## VI. CONCLUSIONS

In this paper we have presented a model which enables us to explain the geometry dependence of the complicated flux distributions obtained on partly irradiated thin films by the HRF technique. The model is based on the flux distribution in the critical state, where the Meissner currents have reached the value $j_c$ everywhere in the sample.

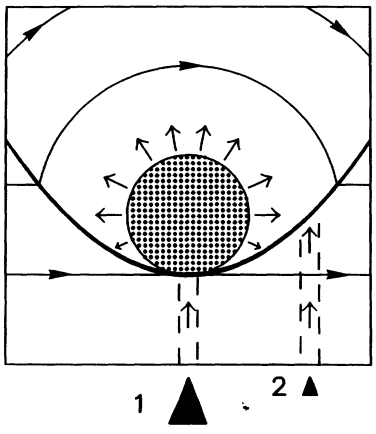


FIG. 8. Schematical drawing of the flux motion in the situation presented in Fig. 1. The vortices always move perpendicular to the current lines as indicated by the open arrows. Many more flux lines penetrate the sample through channel 1 than through channel 2. This is indicated by solid arrows of different size pointing into the direction of flux motion at the bottom of the drawing.

In this ideal critical state, there is only *one* constant critical current density flowing parallel to the sample edges. Therefore, in general, the current paths cannot be closed without forming sharp bends which are imposed by the sample geometry. This leads to the appearance of characteristical lines which were labeled as $d^+$ lines and are clearly visible by magneto-optics.

In addition to these $d^+$ lines, there are defects and edges where two regions with different critical current densities are separated, e.g., by the sample edges or boundaries separating two qualitatively different superconductors. This fact, too, forces the current lines to form sharp bends in order to satisfy the condition of continuous current flow. This again leads to the appearance of characteristical lines at the loci where the value of the critical current density changes, which were labeled $d^-$ lines throughout this work.

Important differences between the $d^+$ lines and the $d^-$ lines are listed below.

(1) The $d^-$ lines are located at edges which cannot only form the outer bounds of the sample but also boundaries within the sample separating regions with different critical current densities. Thus, the $d^-$ lines are a characteristic feature of the local sample geometry.

(2) The location of the $d^+$ lines is determined by the whole sample geometry. In particular, differences in the critical current densities in different regions of the sample contribute strongly to the appearance of the $d^+$ lines. So, the $d^+$ lines reflect the magnetic behavior of the entire sample.

(3) The flux lines are not able to cross the $d^+$ lines. This follows from the flux motion towards and away from these lines while enhancing or, respectively, reducing the external magnetic field. Thus, the $d^+$ lines divide the superconductor into independent areas of flux motion and determine a skeleton of the flux behavior.

To describe the properties of the $d^+$ and the $d^-$ lines in more detail, the line intensity factor $K_l$ which is given by the angle $\vartheta$ enclosed by the current lines at the bending points, $K_l = 2\cos\vartheta/2$, was introduced. Different values of $K_l$ lead to different widths $\Delta x_M$ of the Meissner phase in magneto-optically detected flux distributions in thin films, since $\Delta x_M \sim \exp[-(2/K_l)(H_{\rm ext}/H_c)]$. This yields for the full penetration field $H^* \approx K_l \ln(a/d)$, where $a$ is half the width and $d$ the thickness of the sample. The good visibility of the $d^+$ and the $d^-$ lines in thin film samples at high magnetic fields is due to the occurrence of logarithmic infinities of the magnetic flux density $B_z$ at these lines in thin samples, in contrast to bulk material where the $d^+$ and $d^-$ lines cannot be observed so easily. However, the characteristic features of the $d^+$ and $d^-$ lines mentioned above apply also to bulk samples.The $d^+$ and the $d^-$ lines do not change their position or their $K_l$ values while lowering or reversing the external magnetic field, although the magneto-optically detected intensities of the $d^+$ and $d^-$ lines are reversed in the remanent state. Since the $d^+$ lines depend on the $d^-$ lines, it is possible to determine the differences in the critical current densities which are due to anisotropy, irradiation, defects, or weak

links, etc.

At small defects present in the sample, the flux motion which takes place perpendicular to the current lines becomes visible in the images obtained by the HRF technique. The observed flux distribution agrees very well with the current distribution deduced from the model presented in this work.

## ACKNOWLEDGMENTS

The authors wish to thank W. Andrä, A. Hubert, E. H. Brandt, A. Forkl, V. V. Vlasko-Vlasov, A. A. Polyanskii, V. I. Nikitenko, and L. A. Dorosinskii for helpful and stimulating discussions. The authors are indebted to B. Roas (Siemens AG), M. Leghissa, M. Kraus, G. Saemann-Ischenko (University of Erlangen), P. Keppler, B. Ludescher, and E. Lutkat (MPI Stuttgart) for the sample preparation, the heavy-ion irradiation, and their experimental assistance. One of us (M.V.I.) is grateful to Alexander-von-Humboldt-Stiftung for financial support. Part of this work was financially supported by the Bundesministerium für Forschung und Technologie and the Bayerische Forschungsstiftung (FORSUPRA). This is gratefully acknowledged.

* Permanent address: Institute of Solid State Physics, Russian Academy of Sciences, Chernogolovka, 142432 Moscow distr., Russian Federation.

† Present address: Free University of Amsterdam, De Boelelaan 1081, 1081 HV Amsterdam, The Netherlands.

[1] H. Kirchner, Phys. Lett. **26A**, 651 (1969).

[2] R. P. Huebener, *Magnetic Flux Structures in Superconductors* (Springer, New York, 1979).

[3] Th. Schuster, M. R. Koblischka, N. Moser, B. Ludescher, and H. Kronmüller, Cryogenics **31**, 811 (1991).

[4] N. Moser, M. R. Koblischka, B. Gegenheimer, H. Kronmüller, and H. Theuss, Physica (Amsterdam) C **159**, 117 (1989).

[5] M. V. Indenbom, N. N. Koleshnikov, M. P. Kulakov, A. A. Polyanskii, N. F. Vershinin, and V. K. Vlasko-Vlasov, Physica (Amsterdam) C **166**, 486 (1990).

[6] L. A. Dorosinskii, M. V. Indenbom, V. I. Nikitenko, Yu. A. Ossip'yan, A. A. Polyanskii, and V. K. Vlasko-Vlasov, Physica (Amsterdam) C **203**, 149 (1992).

[7] L. T. Baczewski, K. Piotrowski, R. Szymczak, H. Szymczak, and A. P. Malozemoff, Physica (Amsterdam) C **175**, 363 (1991).

[8] D. Glatzer, A. Forkl, H. Theuss, H.-U. Habermeier, and H. Kronmüller, Phys. Status Solidi B **170**, 549 (1992).

[9] A. A. Polyanskii, L. A. Dorosinskii, M. V. Indenbom, V. I. Nikitenko, Yu. A. Ossip'yan, and V. K. Vlasko-Vlasov, J. Less-Common Met. **164-165**, 1300 (1990).

[10] H. Theuss, A. Forkl, and H. Kronmüller, Physica (Amsterdam) C **190**, 345 (1992).

[11] M. V. Indenbom, A. Forkl, H.-U. Habermeier, and H. Kronmüller, J. Alloys Comp. **195**, 499 (1993).

[12] E. H. Brandt, M. V. Indenbom, and A. Forkl, Europhys. Lett **22**, 735 (1993).

[13] P. Brüll, D. Kirchgässner, and P. Leiderer, Physica (Amsterdam) C **182**, 339 (1991).

[14] V. K. Vlasko-Vlasov, L. A. Dorosinskii, M. V. Indenbom, V. I. Nikitenko, A. A. Poyanskii, and R. L. Prozorov, Supercond. Phys. Chem. Tech. **5**, 2017 (1992).

[15] Th. Schuster, M. R. Koblischka, N. Moser, B. Ludescher, and H. Kronmüller, Physica (Amsterdam) C **179**, 269 (1991).

[16] Th. Schuster, M. R. Koblischka, H. Kuhn, M. Glücker, B. Ludescher, and H. Kronmüller, J. Appl. Phys. **74**, 3307 (1993).

[17] M. R. Wertheimer and J. le G. Gilchrist, J. Phys. Chem. Solids **28**, 2509 (1967).

[18] V. Bujok, P. Brüll, J. Boneberg, S. Herminghaus, and P. Leiderer, Appl. Phys. Lett. **63**, 412 (1993).

[19] D. J. Frankel, J. Appl. Phys. **50**, 5402 (1979).

[20] M. Däumling and D. C. Larbalestier, Phys. Rev. B **40**, 9350 (1989).

[21] L. W. Conner and A. P. Malozemoff, Phys. Rev. B **43**, 402 (1991).

[22] P. N. Mikheenko and Yu. E. Kuzovlev, Physica (Amsterdam) C **204**, 229 (1993).

[23] W. T. Norris, J. Phys. D **3**, 489 (1970).

[24] A. M. Campbell and J. E. Evetts, *Critical Currents in Superconductors* (Taylor & Francis, London, 1972), p. 71.

[25] K.-H. Greubel, E. Gmelin, N. Moser, Ch. Mensing, and L. Walz, Cryogenics **30**, 457 (1990).

[26] B. Ludescher, Th. Schuster, M. R. Koblischka, N. Moser, and H. Kronmüller, Laser und Optoelektronik **23**, 54 (1991).

[27] M. R. Koblischka, N. Moser, B. Gegenheimer, and H. Kronmüller, Physica (Amsterdam) C **166**, 36 (1990).

[28] A. Forkl, H.-U. Habermeier, B. Leibold, T. Dragon, and H. Kronmüller, Physica (Amsterdam) C **180**, 155 (1991).

[29] C. Thomsen, M. Cardona, B. Gegenheimer, R. Liu, and A. Simon, Phys. Rev. B **37**, 9860 (1988).

[30] B. Roas, G. Endres, and L. Schultz, Appl. Phys. Lett. **53**, 1557 (1988).

[31] Th. Schuster, M. R. Koblischka, H. Kuhn, M. Leghissa, M. Lippert, and H. Kronmüller, Physica (Amsterdam) C **196**, 373 (1992).

[32] H. A. M. van den Berg, J. Appl. Phys. **60**, 1104 (1986).

[33] D. A. Brawner, N. P. Ong, and Z. Z. Wang, Nature **358**, 567 (1992).

[34] Th. Schuster, H. Kuhn, M. R. Koblischka, H. Theuss, H. Kronmüller, M. Leghissa, M. Kraus, and G. Saemann-Ischenko, Phys. Rev. B **47**, 373 (1993).

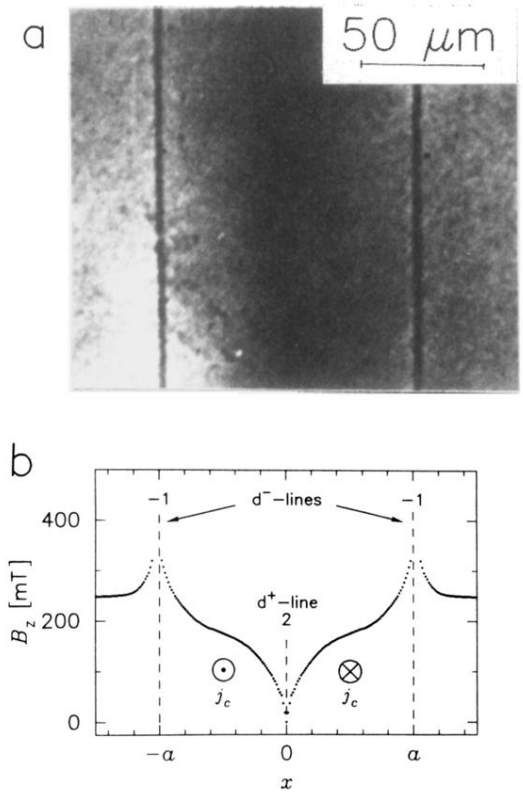


FIG. 2. (a) Direct observation of the flux distribution in a long thin superconducting strip at an external magnetic field of $\mu_0 H_{\text{ext}} = 246$ mT. The observation temperature is $T = 5$ K. The dark lines indicate the sample edges. (b) Flux-density profiles $B_z(x)$ obtained from the image presented in (a); $2a$ denotes the sample width. The influence of the dark lines at the sample edges $a = \pm 0.5$ on the flux density profiles is neglected. The position of the $d^+$ line in the middle of the sample and of the $d^-$ lines at the sample edges and their values $K_l = 2$ and $K_l = -1$, respectively, are indicated. In addition, the direction of flow of the critical current density $j_c$ in each half of the sample is marked by $\odot$ for the direction of flow out of the plane of drawing and by $\otimes$ for the direction of flow into this plane.

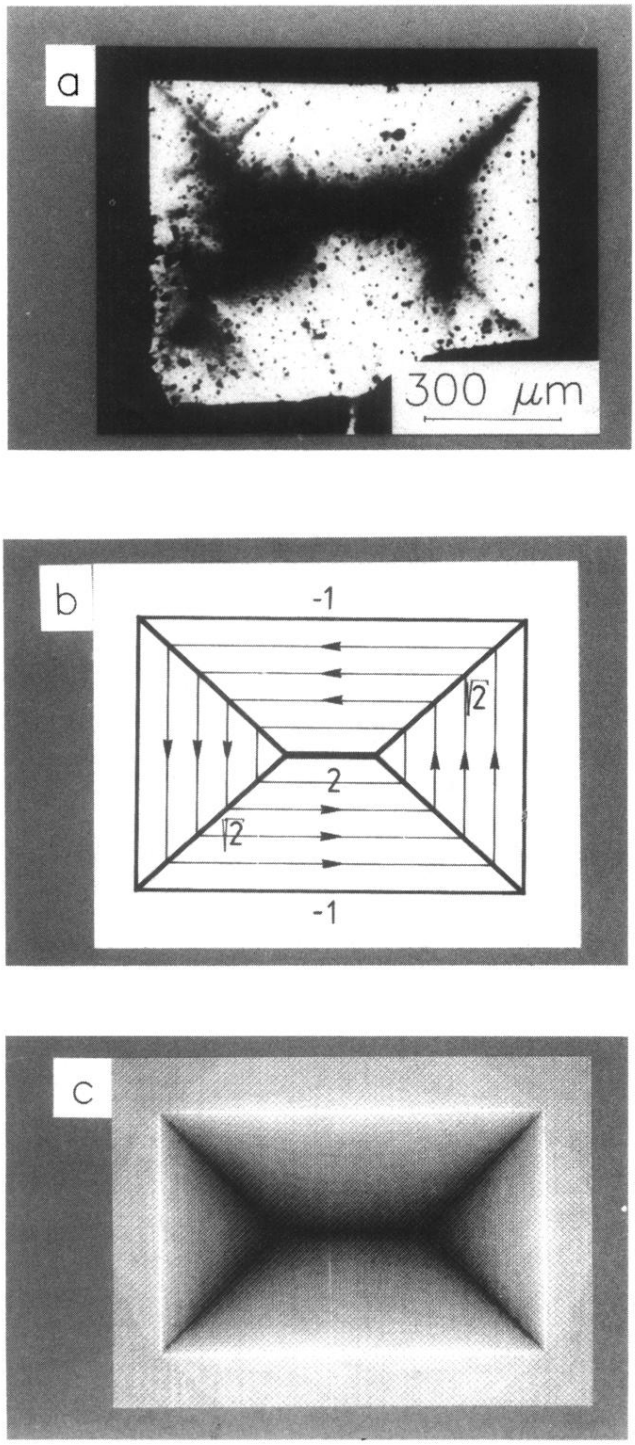


FIG. 3. (a) Flux distribution obtained on a nearly rectangular DyBCO single crystal at an external magnetic field of $\mu_0 H_{\text{ext}} = 512$ mT at $T = 5$ K. The magnetic flux penetrates the sample preferably starting from the middle of each sample edge thus leading to the formation of a Meissner phase shaped as a double $Y$. (b) Current distribution in a rectangular sample. Again, the arrows indicate the direction of flow of the constant current density symbolized by equidistant current lines. The numbers indicate the values of $K_l$ of the respective $d$ lines. The different $K_l$ values for the $d^+$ lines in the center of the sample and along the bisection lines are symbolized by a variable linewidth. (c) Flux distribution calculated from the current distribution presented in (b) via the Biot-Savart law.

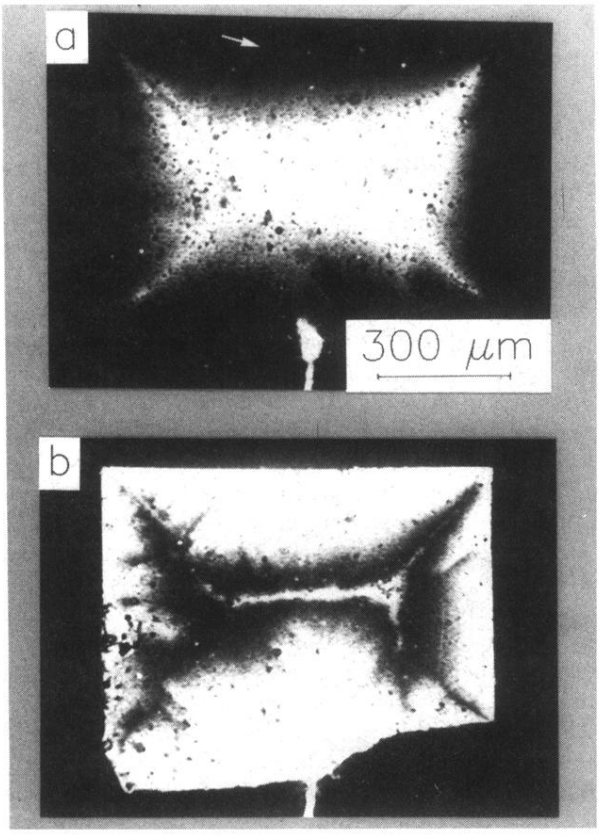


FIG. 4. Remanent state of the DyBCO single crystal presented in Fig. 3(a). (a) Remanent state after applying an external field of $\mu_0 H_{\text{ext}} = 512$ mT and subsequently lowering to 0 mT. In the remanent state the $d^+$ line is imaged bright, whereas the $d^-$ line (white arrow) at the sample edge is hardly visible. (b) Flux distribution obtained from the remanent state presented in (a) while applying an external magnetic field of $\mu_0 H_{\text{ext}} = -300$ mT in reverse direction. The $d^+$ line with the shape of a double $Y$ is clearly visible as a bright line in the center of the sample.

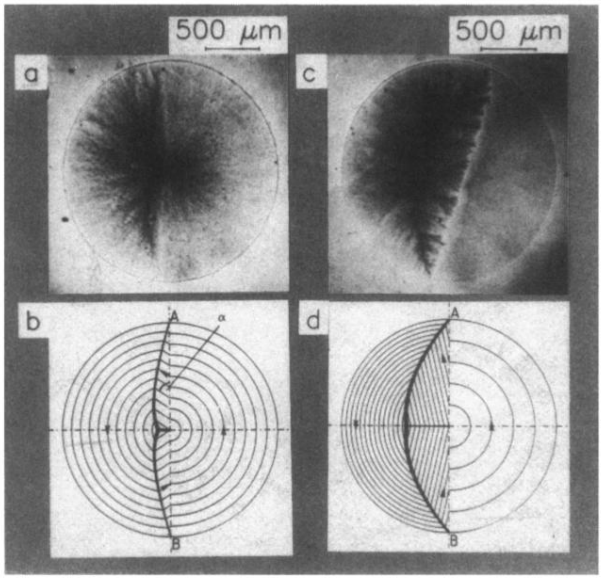


FIG. 5. (a) Flux distribution obtained from a partly irradiated YBCO thin film at an external magnetic field of $\mu_0 H_{\mathrm{ext}} = 273$ mT. The left part of the film was irradiated with 1.0-GeV lead ions at a fluence of $\phi t = 9.0 \times 10^{10}$ ions/cm$^2$. The asymmetric flux distribution due to the irradiation-induced enhancement of the critical current density is clearly visible. (b) Current distribution in the thin film presented in (a). The constant critical current density in each half of the sample is symbolized by equidistant concentric circles. The thickness of the $d^+$ line indicates the value of $K_l$ which becomes a maximum at the center of the $d^+$ line. (c) Flux distribution obtained from a YBCO thin film at an external magnetic field of $\mu_0 H_{\mathrm{ext}} = 273$ mT. The left half of the sample was irradiated with 1.0-GeV lead ions at a fluence of $\phi t = 30.0 \times 10^{10}$ ions/cm$^2$ . The difference in the critical current densities in both parts is apparently larger than in the case presented in (a). (d) Current distribution in the sample presented in (c).

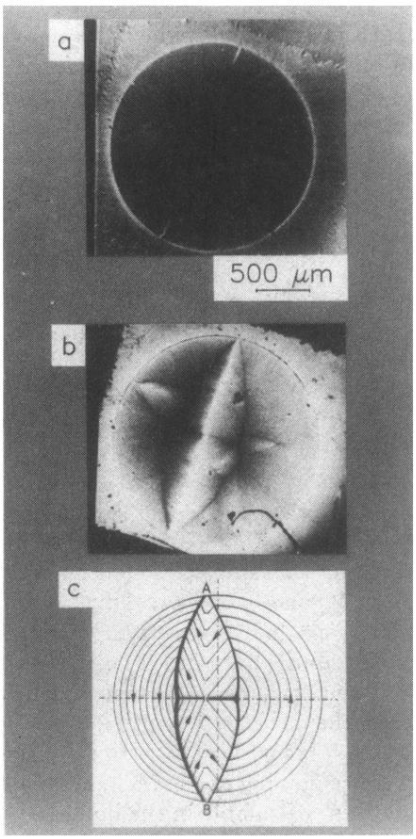


FIG. 6. (a) Flux distribution in an oxygen irradiated YBCO thin film at an external magnetic field of $\mu_0 H_{ext} = 27$ mT. The left half was irradiated at a fluence of $\phi t = 6.0 \times 10^{14}$ ions/cm$^2$. The flux penetration along the division line between the irradiated and unirradiated part of the sample due to mechanical tension in the boundary region is clearly visible. (b) The same sample at an external magnetic field of $\mu_0 H_{ext} = 273$ mT. The formation of the $d^+$ lines due to the irradiation and due to the defect in the upper left part of the sample are clearly visible. (c) Current distribution of the situation presented in (b).